Journal of ELECTRONIC MATERIALS, Vol. 45, No. 5, 2016
DOI: 10.1007/s11664-015-4313-4

Facile Fabrication of Platinum Nanodots Assembly Core–Silica Shell Nanosystems

DIANA KOSTYUKOVA[1] and HYOJONG YOO[1,2]

1.—Department of Chemistry, Hallym University, Chuncheon, Gangwon-do 24252, Republic of Korea. 2.—e-mail: hyojong@hallym.ac.kr

Nanosystems using a platinum (Pt) nanodots assembly (multi-Pt nanoparticles, m-Pt) as the core and silica (SiO_2) shells were successfully synthesized as m-Pt@SiO_2 spherical nanoparticles (NPs) and m-Pt@SiO_2 nanochains (NChs) by a reverse microemulsion (water-in-oil)-based method. The kinetically controlled reduction of K_2PtCl_4 by the Brij35 surfactant within reverse micelles, followed by condensation of tetraethyl orthosilicate, led to the formation of multi-Pt nanodots core–silica shell systems. The reduction kinetics for the growth of core–shell systems was studied in both the presence of reducing agents such as ascorbic acid, glucose, and ethylene glycol and in the absence of supplementary agents, as well as the variation of water-to-surfactant ratio. To assemble Pt NPs within a one-dimensional SiO_2 matrix, we attempted to grow Pt NPs *in situ* while the SiO_2 materials grew one-dimensionally in a modified microemulsion system. By changing the pH of the reaction media or using highly concentrated ethylene glycol in the synthetic approach, we successfully synthesized m-Pt@SiO_2 NChs.

Key words: Platinum nanodots assembly, silica, core–shell structure, reverse microemulsion

INTRODUCTION

Great scientific and engineering interest in the research of nanoparticles assembly has arisen within the last two decades.[1–5] The chemical and physical properties of nanoparticles assembly heavily depend on the components and structural properties of the nanoparticles, including the size, shape and distribution of the arranged nanoparticles.[6–8] The colligative properties of nanoparticles assembly are significantly affected by the distances and interactions among the nanoparticles as basic elements.[9] By understanding the size- and distribution-related changes in such systems, advanced materials could be developed together with many innovative technologies. Different technological areas in the fields of electronics,[10–13] diagnostics,[14] catalysis,[15–17] and medicine[18–20] could make use of the exciting properties of the emerging nanoparticles.

(Received October 6, 2015; accepted December 17, 2015; published online January 4, 2016)

One of the methods of assembling metallic nanoparticles is to surround them with an outer media with inorganic oxide materials such as silica (SiO_2). Silica-coated nanomaterials have a wide range of potential applications in catalysis,[21–24] electronics,[25–31] and biomedical applications.[32,33] Recently, an expedient synthetic method for highly spherical nanoparticles with gold (Au) nanodots assembly as the core and silica shell was developed by our research group.[34] By using a reverse (water-in-oil) microemulsion, silica-encapsulated Au nanodots with diameters of 2–5 nm were successfully prepared in a controllable fashion. The silica shell could be further etched in a simple treatment to generate the Au nanodots core–mesoporous silica shell nanoparticles in an aqueous medium.[35] These were novel and simple synthetic approaches for generating functional hybrid Au-silica nanomaterials by encapsulating Au nanoparticles assembly within a silica matrix.

Interest in platinum (Pt)-based nanoparticles assembly is greatly intensified by the potential to

increase the unique properties of pure Pt nanomaterials.[36–40] Moreover, it is a valuable focus of research to assemble Pt nanoparticles effectively in confined areas. Nanosystems composed of Pt nanoparticles cores and silica shells could improve the stability of Pt nanoparticles. The outer shells could isolate the catalytically active nanoparticle cores and prevent the possibility of Pt sintering during catalytic reactions at high temperatures. In addition, the synergistic effects of the metal-support interfaces could be maximized in situations in which such interfaces are important in catalytic performances.[41–43]

Herein we report the synthesis of multi-Pt (m-Pt) nanodots assembly core–silica shell nanosystems of spherical m-Pt@SiO_2 nanoparticles (NPs) and m-Pt@SiO_2 nanochains (NChs). The reverse microemulsion synthesis method was used, and the Pt nanoparticles and the silica layer were grown *in situ* in the modified microemulsion. The kinetically controlled reduction of K_2PtCl_4 by the Brij35 surfactant and supplementary reducing agents of ascorbic acid (AA), glucose, and ethylene glycol (EG) within the reverse micelles, followed by the condensation of tetraethyl orthosilicate (TEOS), generated m-Pt nanodots assembly core–silica shells nanosystems.

EXPERIMENTAL DETAILS

Reagents

Polyoxyethylene glycol dodecyl ether [$(C_2H_4O)_{23}C_{12}H_{25}OH$, Brij35, Acros Organics], tetraethylorthosilicate (TEOS, 99%, Sigma-Aldrich), potassium tetrachloroplatinate(II) (K_2PtCl_4, Sigma-Aldrich), ammonium hydroxide (NH_4OH, 28–30 wt.% ammonia, Sigma-Aldrich), cyclohexane (C_6H_{12}, 99%, Sigma-Aldrich), *n*-hexanol (C_6H_5OH, 98%, Sigma-Aldrich), L-ascorbic acid ($C_6H_8O_6$, 99+%, Sigma-Aldrich), D-(+)-glucose ($C_6H_{12}O_6$, ACS reagent Sigma-Aldrich), ethylene glycol ($HOCH_2$-CH_2OH, anhydrous, 99.8%, Sigma-Aldrich), HCl, HNO_3, acetone, and ethyl alcohol were used as received. All stock solutions were freshly prepared before each reaction. Prior to use, all glassware was washed with aqua regia (3:1 ratio by volume of HCl and HNO_3; *caution: aqua regia is highly toxic and corrosive and must be handled in a fume hood with proper personal protection equipment*) and rinsed thoroughly with nanopure water. Abbreviations used: EG = ethylene glycol; AA = ascorbic acid.

Synthesis of Spherical m-Pt@SiO_2 Nanoparticles (m-Pt@SiO_2 NPs)

For the synthesis of m-Pt@SiO_2 NPs, we modified the synthetic method which was used to create the multi-Au@SiO_2 NPs.[34,35] The reverse microemulsion was prepared by mixing Brij35 (2.0 g), cyclohexane (7.7 mL) and *n*-hexanol (1.6 mL), and completely dissolving them via sonication. Next, 0.1 mL of 0.1 M K_2PtCl_4 (*aq.*) was added to the reverse microemulsion and the mixture was sonicated for 30 min at room temperature. This was followed by the addition of 0.2 mL of 0.1 M AA (*aq.*) solution; the mixture was sonicated for 30 min. Next, 50 μL of tetraethyl orthosilicate (TEOS) and 500 μL of 14.8 M NH_4OH (*aq.*) were sequentially added to the reverse microemulsion while stirring for 30 min, and the reaction mixture was further stirred at room temperature for 12 h. After the completion of the reaction, 20 mL of acetone was added to destabilize the microemulsion system. The synthesized nanoparticles (m-Pt@SiO_2 NPs) were acquired by centrifugation at 2000 rpm for 5 min, and then purified by repeated washing in ethanol (three times) and centrifugation (13,500 rpm, 5 min). In a separate reaction, aqueous solutions of different concentration of AA (none, 0.1, 0.5, 1.0, and 2.0 M), and other reducing agents such as glucose (0.1 M) and EG (0.1, 1.0, 2.0, and 18.0 M) solutions were added to the reverse microemulsion system after adding K_2PtCl_4 (*aq.*).

Structural Control of m-Pt@SiO_2 NPs

The concentration of the K_2PtCl_4 was varied in the synthesis (0.001, 0.01, 0.1, and 0.5 M) of K_2PtCl_4 (*aq*), with other original parameters held constant. To change the water-to-surfactant ratio in the reverse microemulsion, 0.02 ml of a 0.5 M, 0.1 mL of a 0.1 M, 1 mL of a 0.01 M K_2PtCl_4 [*aq.*; with the same moles of Pt^{2+} precursor (0.01 mmol)] were used for each trial. Size distributions of m-Pt@SiO_2 NPs synthesized were checked in each trial. For the investigation of high-temperature treatment of the synthesized m-Pt@SiO_2 NPs, the pre-synthesized m-Pt@SiO_2 NPs were redispersed in nanopure water (1 mL) and heated at 90°C for 12 h and at 180°C for 36 h by using Teflon-lined stainless steel autoclave under autogenic pressure developed inside the Teflon liners. The reaction mixture was cooled to room temperature, centrifuged (13,500 rpm, 5 min), and stored in ethanol for the further use.

Synthesis of Platinum Nanodots in Brij35 (*aq.*) Solution

For the synthesis of platinum nanodots in Brij35 (*aq.*) solution, the reverse microemulsion was prepared by adding Brij35 (2.0 g), cyclohexane (7.7 mL) and *n*-hexanol (1.6 mL), and completely dissolving via sonication. 0.1 mL of 0.1 M K_2PtCl_4 (*aq.*) was added to the reverse microemulsion and the mixture was sonicated for 30 min at room temperature. This was followed by the addition of 500 μL of 14.8 M NH_4OH (*aq.*), and the reaction mixture was further stirred at room temperature for 12 h. After the completion of the reaction, 20 mL of acetone was added to destabilize the microemulsion system. The synthesized nanoparticles were acquired by centrifugation at 2000 rpm for 5 min, and then purified

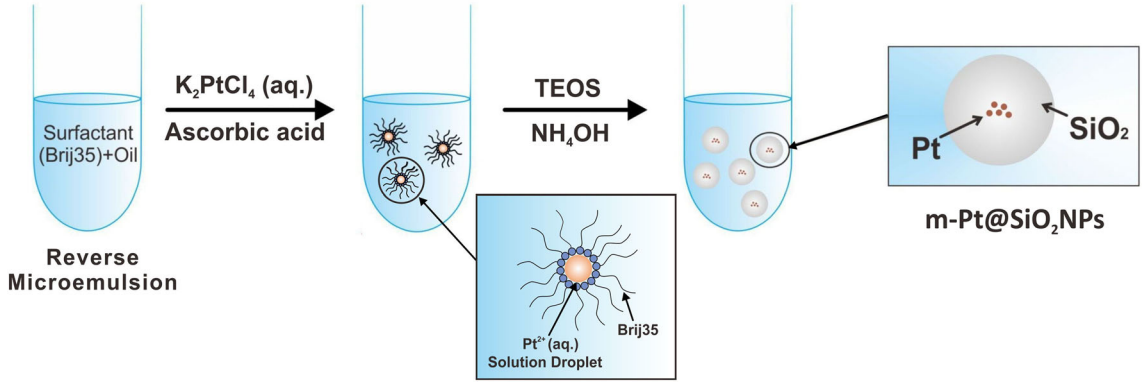

Scheme 1. Synthesis of the m-Pt@SiO_2 NPs.

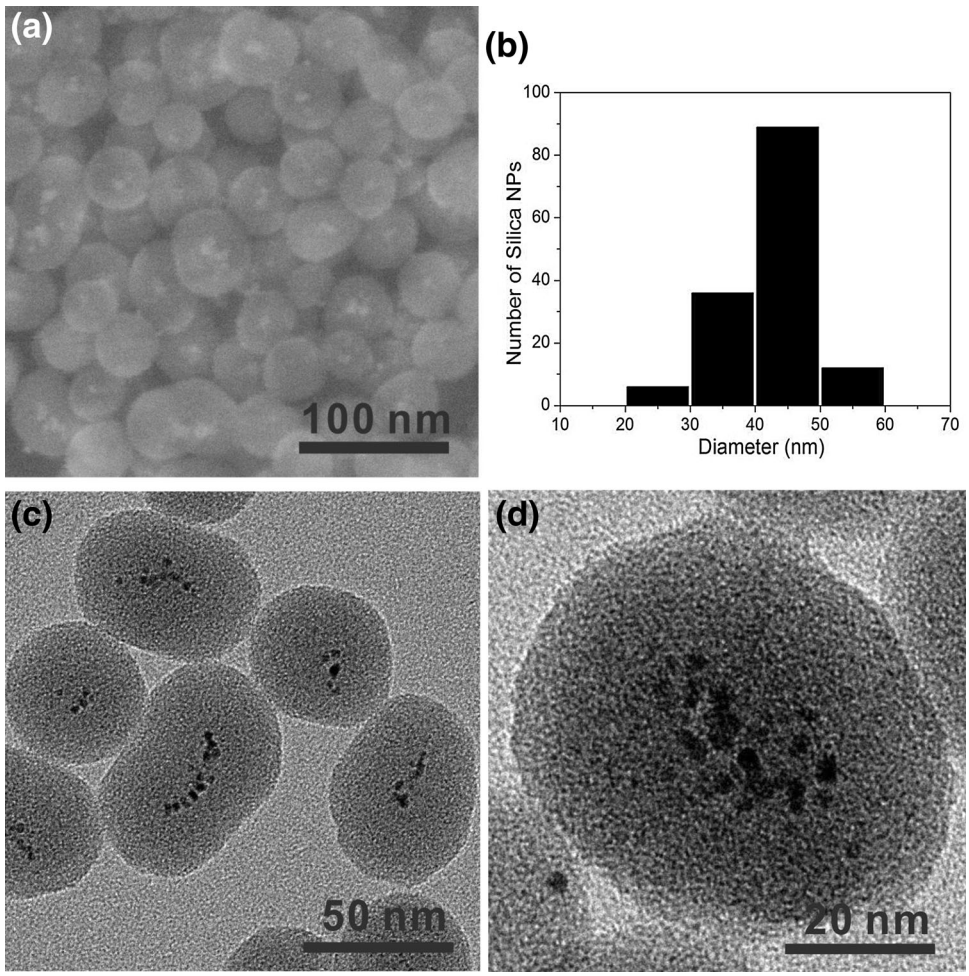

Fig. 1. (a) Scanning electron microscopy (SEM) image of m-Pt@SiO_2 NPs; (b) Size distribution of m-Pt@SiO_2 NPs; (c) and (d) Transmission electron microscopy (TEM) images of m-Pt@SiO_2 NPs.

by repeated washing in ethanol (three times) and centrifugation (13,500 rpm, 5 min).

Synthesis of m-Pt@SiO_2 NChs (Nanochains)

For the synthesis of the m-Pt@SiO_2 NChs, 2.0 g of Brij35, 7.7 mL of cyclohexane, and 1.6 mL of *n*-hexanol were completely mixed via sonication. The Pt precursor of 0.1 mL of K_2PtCl_4 (*aq.*; 0.1 M) was added to the reaction mixture and sonicated for 30 min at room temperature. 0.5 mL of 1 M HCl (*aq.*) was added into the reaction mixture and the mixture was sonicated for 30 min. Sequentially, 50

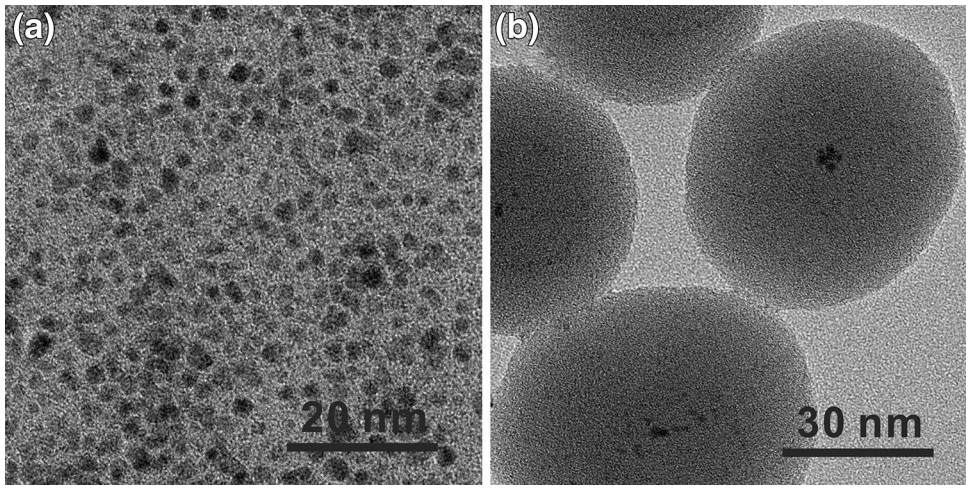

Fig. 2. (a) TEM image of Pt nanoparticles synthesized in Brij35(*aq.*); (b) TEM images of m-Pt@SiO_2 NPs synthesized in Brij35 (*aq*; no other reducing agents were used).

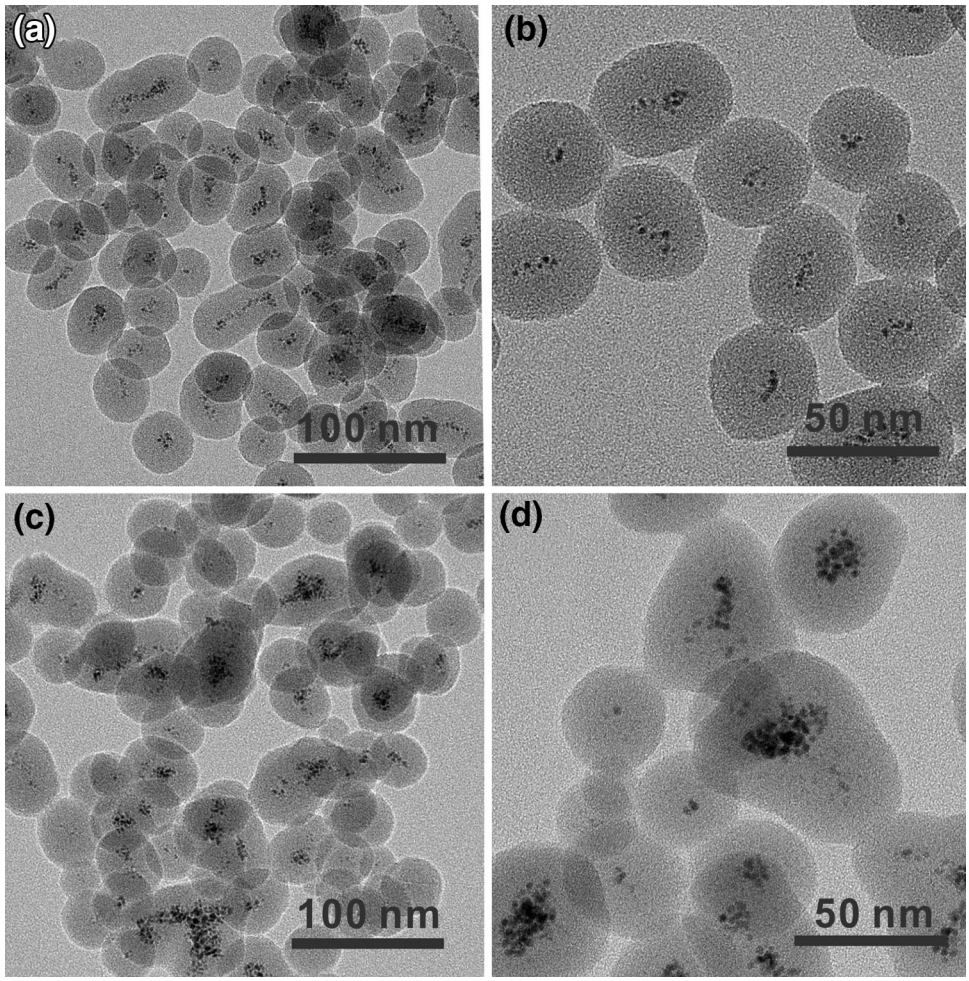

Fig. 3. TEM images of m-Pt@SiO_2 NPs grown using: (a, b) glucose (0.1 M); (c, d) EG (0.1 M), with other original synthesis parameters held constant.

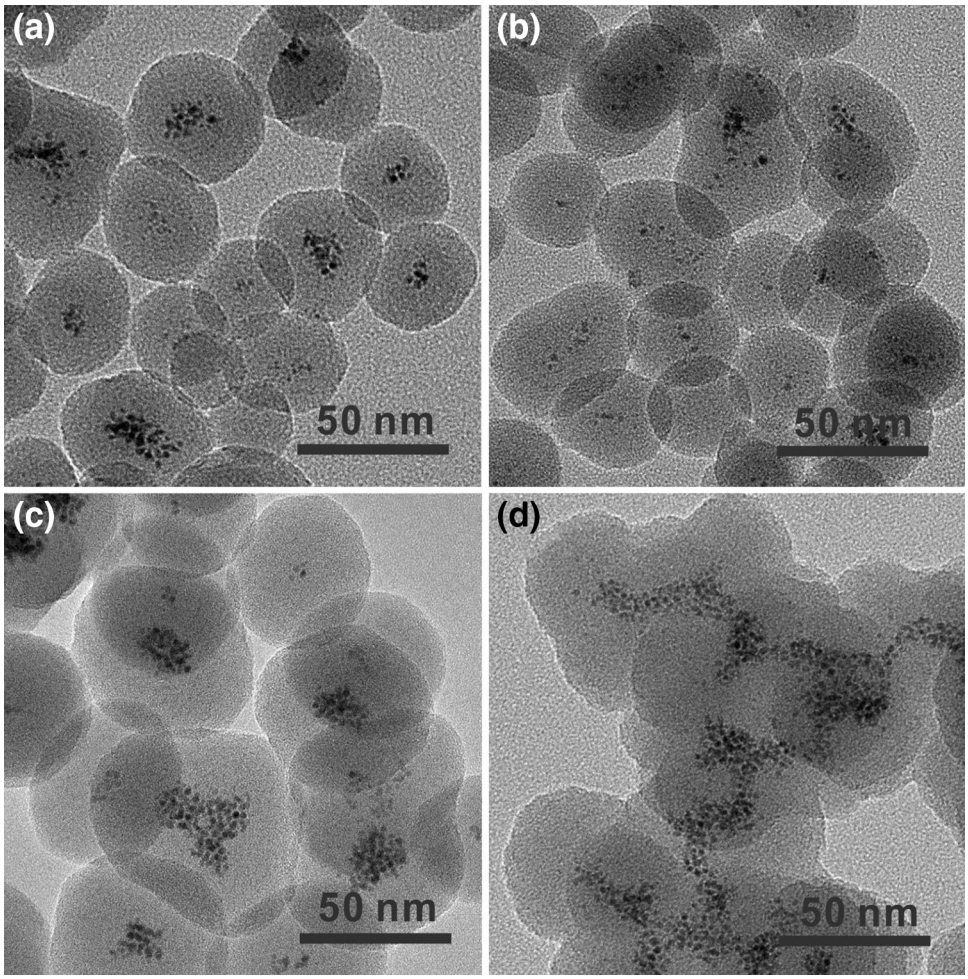

Fig. 4. TEM images of m-Pt@SiO_2 NPs grown using: (a) 0.2 mL of 1 M EG; (b) 0.2 mL of 2 M EG; (c) 0.2 mL of 18.0 M EG, and (d) 1.0 mL of 18.0 M EG, with other original synthesis parameters held constant.

μL of TEOS and 500 μL of 14.8 M NH_4OH (*aq.*) were added to the mixture while stirring for 30 min. The reaction mixture was further stirred at 50°C for 6 h, and the microemulsion system was destabilized by adding 20 mL of acetone. The generated m-Pt@SiO_2 NChs were acquired by centrifugation at 2000 rpm for 5 min, and then were purified by repeated washing in ethanol (three times) and centrifugation (13,500 rpm, 5 min).

Separately, m-Pt@SiO_2 NChs were synthesized by using highly concentrated EG. The reaction mixture consisted of 2.0 g of Brij35, 7.7 mL of cyclohexane, and 1.6 mL of *n*-hexanol and was completely mixed via sonication. 0.1 mL of 0.1 M K_2PtCl_4 (*aq.*) was added to the reverse microemulsion and sonicated for 30 min at room temperature. This was followed by the addition of 2 mL of 18.0 M EG (*aq.*) and sonication of the reaction mixture for 30 min. Next, 50 μL of TEOS and 500 μL of 14.8 M NH_4OH (*aq.*) were sequentially added with stirring, and the reaction mixture was further stirred at room temperature for 12 h. After the completion of the reaction, 20 mL of acetone was added to destabilize the microemulsion system. The synthesized m-Pt@SiO_2 NChs were acquired by centrifugation at 2000 rpm for 5 min, and then purified by repeated washing in ethanol (three times) and centrifugation (13,500 rpm, 5 min).

Characterization

The resulting nanoparticles were imaged via scanning electron microscopy (SEM) using a Hitachi S-4800 (Japan) scanning electron microscope and via field emission transmission electron microscopy (FETEM) using a JEOL JEM-2100F (Japan) instrument. Samples for the TEM analysis were prepared by concentrating the nanoparticle mixture by centrifuging it twice for 3 min at 13,500 rpm. Following this, the particles were resuspended in 100 μL of nanopure water and immobilized from 10 μL portions of the solution on Formvar/Carbon 400 mesh Cu grids.

RESULTS AND DISCUSSION

To synthesize m-Pt@SiO_2 NPs, the reverse-microemulsion system shown in Scheme 1 was employed. For the growth of the Pt nanodots assembly comprising the core, aqueous K_2PtCl_4

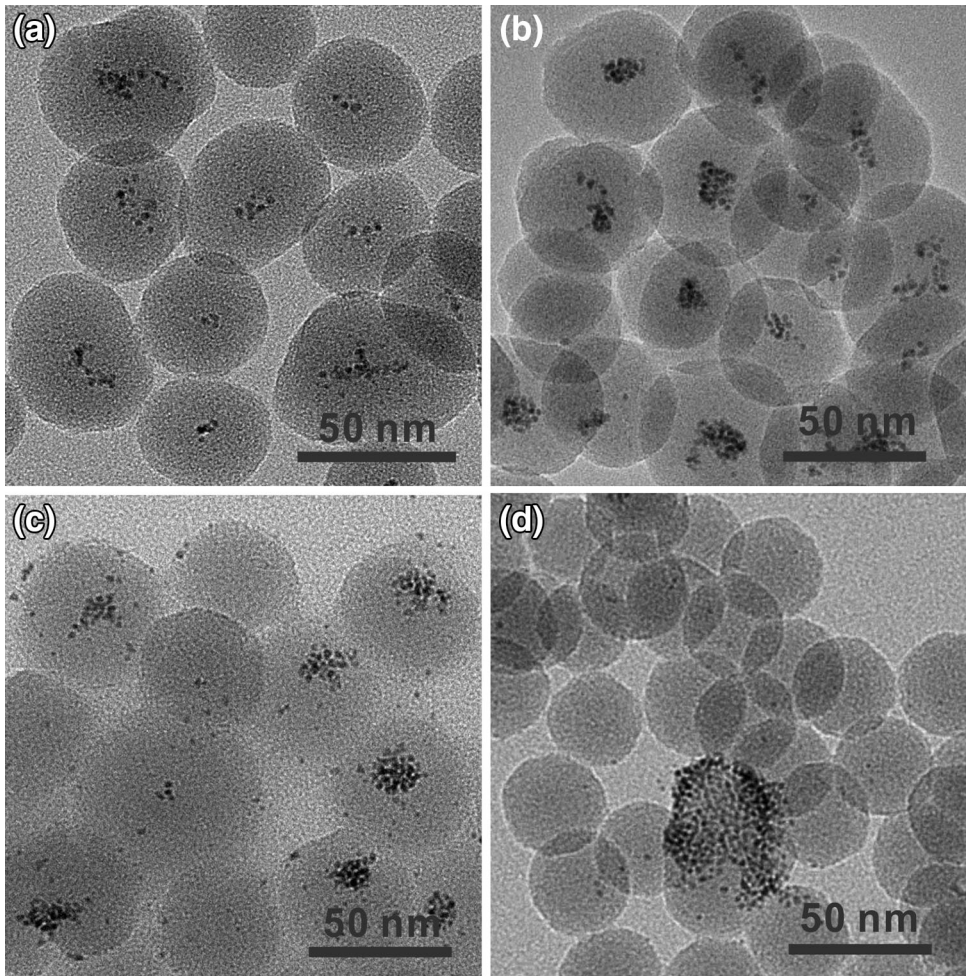

Fig. 5. TEM images of m-Pt@SiO_2 NPs grown using: (a) 0.1 M AA; (b) 0.5 M AA; (c) 1.0 M AA; and (d) 2.0 M AA (*aq*), with other original synthetic parameters held constant.

solution was used as a Pt precursor. AA was added to the system as a supplementary reducing agent for the more complete reduction of Pt^{2+}.

The microemulsion was prepared by completely mixing Brij35, *n*-hexanol, and cyclohexane via sonication. K_2PtCl_4 (*aq.*), AA, TEOS, and NH_4OH were sequentially added into the reverse microemulsion, and the reaction mixture was further stirred at room temperature for 12 h. After the completion of the reaction, acetone was added to destabilize the microemulsion system, and the generated m-Pt@SiO_2 NPs were purified by repeated washing in ethanol and centrifugation. Figure 1a demonstrates the SEM image of the m-Pt@SiO_2 NPs, which clearly shows that the reverse microemulsion system is effective for the formation of the spherical silica morphology with a narrow size distribution. The average diameter of the individual silica nanoparticles is 43.3 ± 5.5 nm (more than 100 silica nanoparticles were evaluated; Fig. 1b). The TEM images of m-Pt@SiO_2 NPs (Fig. 1c and d) exhibit several Pt nanodots within each silica nanoparticle. Almost all Pt nanodots are localized at the center of the silica matrix with narrow nanogaps in the m-Pt@SiO_2 NPs. The Pt nanodots are successfully encapsulated in the silica matrix of generated nanoparticles.

The m-Pt@SiO_2 NPs could be also synthesized in the absence of AA in the reverse-microemulsion system (Fig. 2b). In general, Au^{3+} (*aq.*) was easily reduced in aqueous Brij35 solution without other reducing agents; some anisotropic Au nanoparticles were synthesized with Brij surfactants as reducing and shape-directing agents.[34–36,44–46] In addition, Au nanodots assemblies were successfully synthesized using aqueous Brij35 solution within silica nanoparticles without any other reducing agents.[34] However, $PtCl_4^{2-}$ to Pt(0) shows a lower reduction potential than Au(III) to Au(0) and, in general, requires stronger reducing agents or different reaction conditions (i.e., higher reaction temperatures) to reduce the aqueous Pt(II) ion to Pt(0) metal.[47] In our experimental results, K_2PtCl_4 could be reduced in Brij35 (*aq.*) without supplementary reducing agents to generate Pt nanoparticles of 3–5 nm in diameter at room temperature (Fig. 2a). The

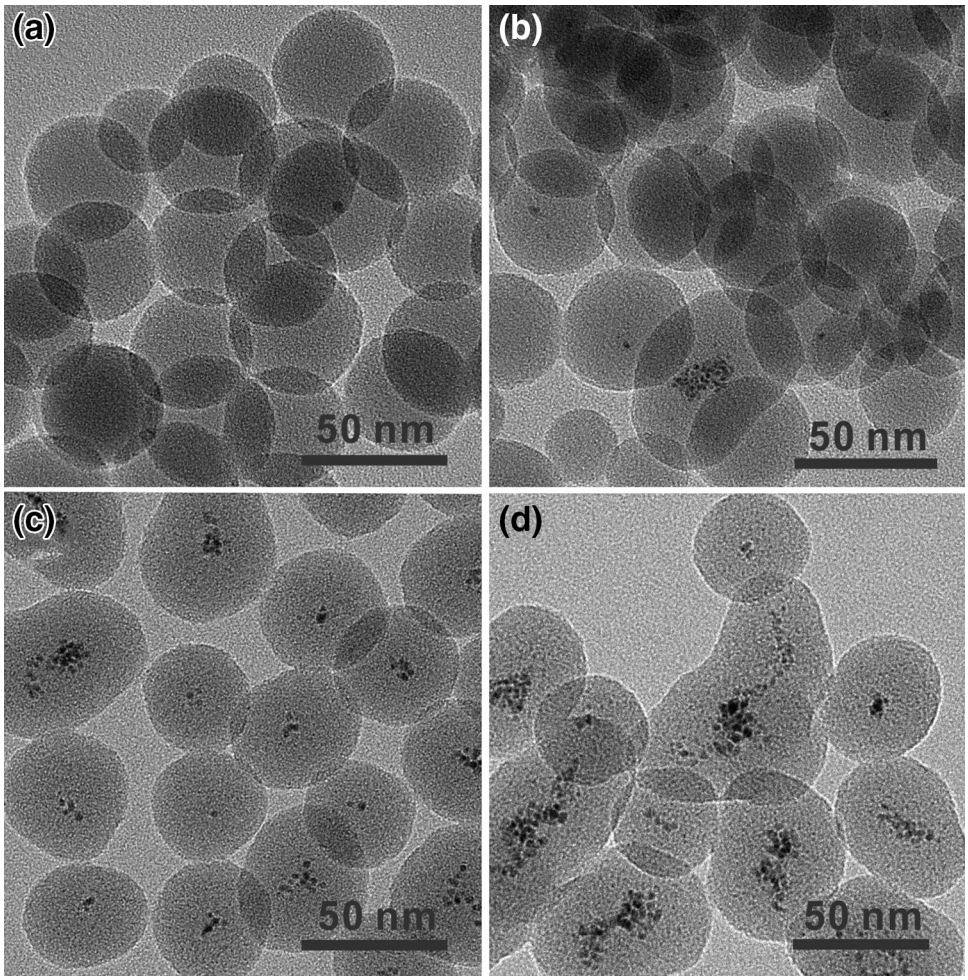

Fig. 6. TEM images of m-Pt@SiO_2 NPs grown with: (a) 0.001 M, (b) 0.01 M, (c) 0.1 M, and (d) 0.5 M K_2PtCl_4 (*aq*), with other original synthetic parameters held constant.

average diameter of the Pt nanodots in m-Pt@SiO_2 NPs is 3.2 ± 1.3 nm (Fig. 1, more than 100 silica nanoparticles were evaluated), which is almost similar to the values evaluated in Pt nanodots synthesized in Brij35 (*aq.*; Fig. 2a) and in m-Pt@SiO_2 NPs without any other reducing agents (Fig. 2b).

The reduction kinetics for the growth of core–shell systems and the synthesized m-Pt@SiO_2 NPs were compared in the reactions using reducing agents such as glucose and ethylene glycol (EG). The Pt nanodots are localized in the center of silica matrix, regardless of the supplementary reducing agents (Fig. 3).

The average diameters of Pt nanodots in each m-Pt@SiO_2 NP are 3.1 ± 1.1 nm (with glucose, Fig. 3a and b) and 3.2 ± 1.1 nm (with EG, Fig. 3c and d), which do not show any change from the value of 3.2 ± 1.3 nm shown in Fig. 1 (with AA). The average diameters of m-Pt@SiO_2 NPs grown with glucose are 36.2 ± 4.3 nm (with glucose, Fig. 3a and b) and 45.2 ± 5.8 nm (with EG, Fig. 3c and d), which are also similar to the value from Fig. 1 (43.3 ± 5.5 nm, with AA). Figure 4 show the TEM images of m-Pt@SiO_2 nanosystems grown using diverse concentrations and volumes of EG. There were almost no differences in the morphologies of synthesized m-Pt@SiO_2 NPs at low concentration [Figs. 3c and d, 4a and b; 0.2 mL of 0.1–2 M EG (*aq.*)] from those synthesized using AA and glucose. However, m-Pt@SiO_2 nanosystems grown with greater amounts of EG [0.2 mL (Fig. 4c) and 1 mL (Fig. 4d) of 18 M EG (*aq.*)] show much bigger sizes (evaluations were made by counting the cross-section diameter). These size and morphological changes might result from the similarity in chemical properties of the Brij35[48] and EG[49–51] structures, which both contain polar –OH functional groups. We speculate that the strong interactions of Brij35 and EG in a reverse microemulsion lead to the changes in the structure of reverse micelles which can be used as a soft template for the growth of formation of m-Pt@SiO_2 NPs.

The effect of AA concentration was investigated (Fig. 5). With increasing the concentration of AA, the diameter of m-Pt@SiO_2 NPs slightly decreased.

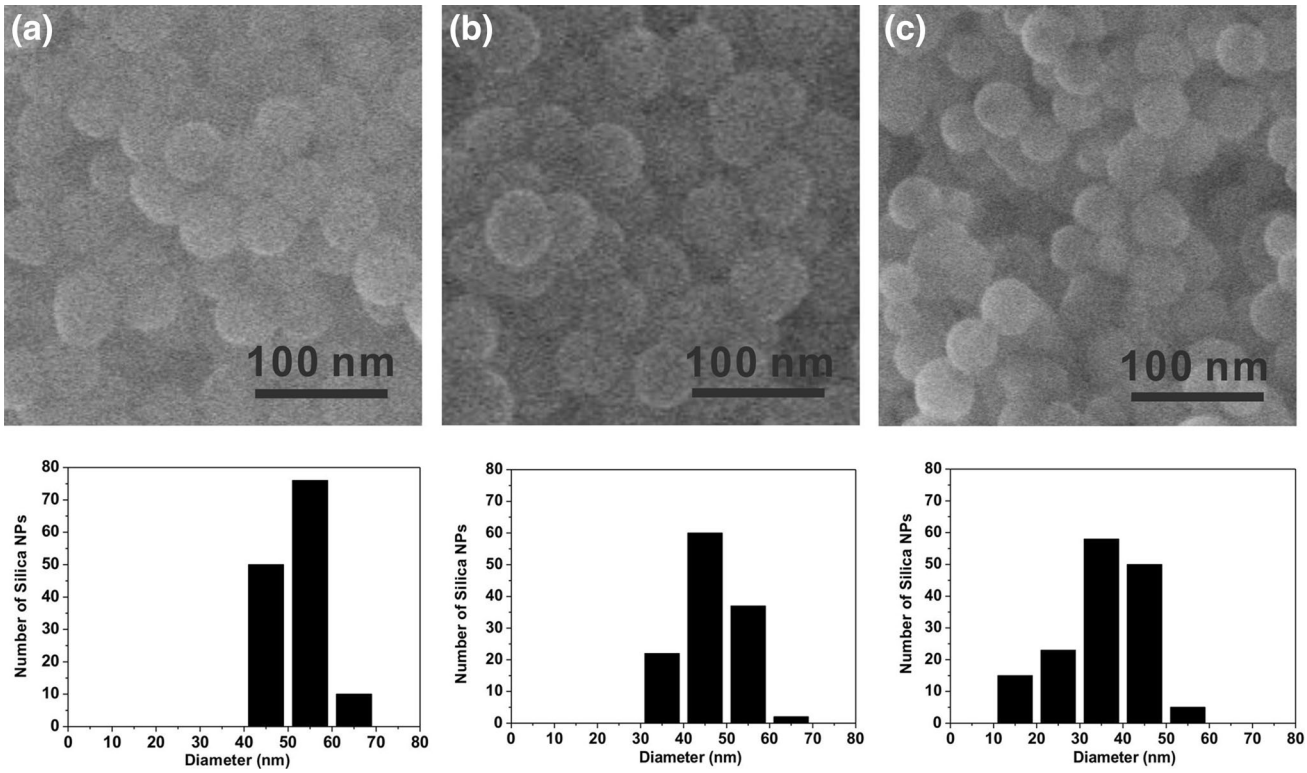

Fig. 7. SEM images of m-Pt@SiO_2 NPs synthesized by varying the water-to-surfactant ratios: (a) 0.02 ml of a 0.5 M, (b) 0.1 mL of a 0.1 M, and (c) 1 mL of a 0.01 M K_2PtCl_4 (*aq*), with the same moles of Pt^{2+} precursor (0.01 mmol) used for each trial; (below) Size distribution of m-Pt@SiO_2 NPs synthesized in each trial.

In Fig. 5a–d, the silica diameters are 43.3 ± 5.4 nm, 46.6 ± 4.6 nm, 42.3 ± 3.3 nm, and 32.3 ± 2.7 nm, respectively. Higher concentrations of H^+ may decrease the amount of OH^-, which is required for TEOS hydrolysis. This deficiency may reduce the growth rate of the synthesized silica nanoparticles, resulting in a smaller size.[34,52] No changes were observed in the size of Pt nanodots with changing AA concentration. Interestingly, as a high amount of AA was used, it was observed that m-Pt nanodots were no longer localized at the center of the silica matrix (Fig. 5c and d). The condensation rate of silica could be decreased with increasing the concentration of AA. The reduction rate of K_2PtCl_4 seemed to be relatively faster than the condensation of TEOS, as the most Pt nanodots could not be eventually organized on the center of the silica matrix (Fig. 5d).

The number and size of Pt nanodots in the structure of m-Pt@SiO_2 NPs could be controlled by varying the concentration of K_2PtCl_4, as demonstrated in Fig. 6. Increasing the concentration of K_2PtCl_4 leads to the formation of, on average, more Pt nanodots within the silica shell (Fig. 6).

To investigate the effect of water on the size of the m-Pt@SiO_2 NPs, the amount of Pt^{2+} ions in the aqueous medium was kept constant during synthesis while the volume of K_2PtCl_4 (*aq*) added to the microemulsion was varied. Figure 7 shows the SEM images of the m-Pt@SiO_2 NPs formed with different water-to-surfactant ratios: the water-to-surfactant ratio was increased by increasing the volume of K_2PtCl_4 (aq.) added. The nanoparticles depicted in Fig. 7 were synthesized with 0.01 mmol of K_2PtCl_4 (*aq*) in different volumes and concentrations. The average diameters of these m-Pt@SiO_2 NPs are 53.0 ± 1.8 (a), 45.1 ± 0.8 (b), and 38.2 ± 2.1 nm (c); as demonstrated in the histograms in Fig. 7 (each m-Pt@SiO_2 NP sample was counted; more than 100 silica nanoparticles from each sample were evaluated). This shows that the size of the m-Pt@SiO_2 NPs decreases with increasing the volume of water, corresponding to an increasing the water-to-Brij35 ratio.[53] While silica NPs grow, silica nuclei form initially, which is followed by the condensation of hydrolyzed TEOS on the surfaces of the silica nuclei. The number of seeding silica nuclei that formed in the water phase of the reverse microemulsion can be the key factor for the size control of the silica NPs. As the water concentration increased, more silica nuclei can be generated within the water drops. Hydrolyzed TEOS can be condensed on a larger number of nuclei than may then lead to the formation of smaller silica NPs.[34,53,54]

To investigate the stability of platinum dots in the m-Pt@SiO_2 NPs and structural changes in the silica matrix, we treated the m-Pt@SiO_2 NPs system with a high-temperature treatment at 90 and 180°C for 12 and 36 h in water, respectively. With heating the investigated system at 90°C for 12 h (Fig. 8a) and

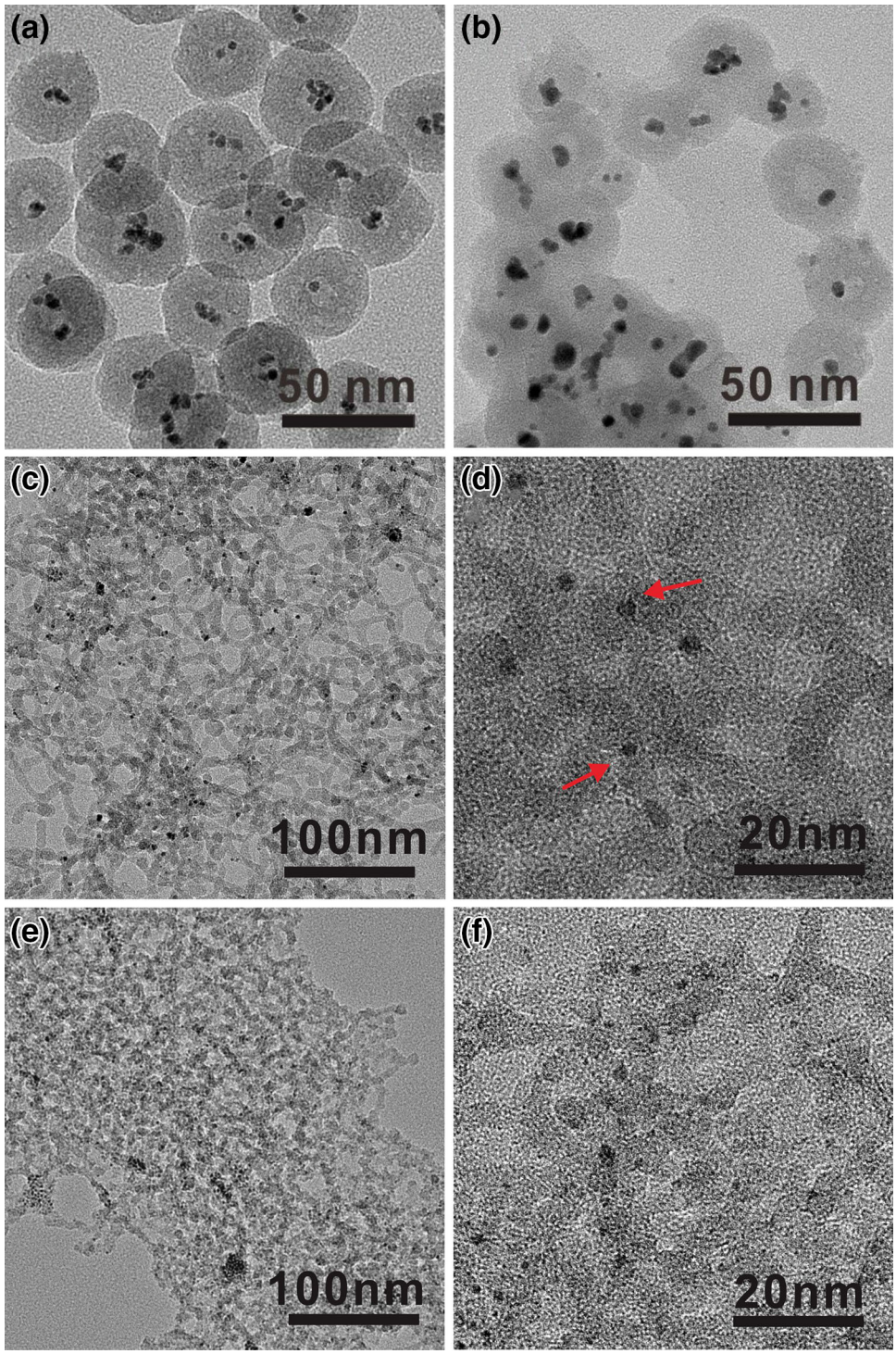

Fig. 8. TEM images of m-Pt@SiO_2 NPs after heating (a) at 90°C and (b) at 180°C in water; (c, d) TEM images of m-Pt@SiO_2 NChs; arrows in (d) indicate Pt nanodots grown within silica nanochains; (e, f) TEM images of m-Pt@SiO_2 NChs grown using 18.0 M EG (*aq.*).

heating at 180°C for 36 h (Fig. 8b), aggregation of Pt nanodots followed by the generation of slightly larger Pt nanodots was observed within the m-Pt@SiO_2 NPs, although the basic spherical morphology of silica was retained under high temperatures.[55] The average diameters of Pt nanodots are 4.1 ± 0.9 (Fig. 8a, under heating at 90°C for 12 h) and 4.3 ± 1.9 nm (Fig. 8b, under heating at 180°C for 36 h), which showed an ~30% increase from the Pt nanodots before heating (3.2 ± 1.3 nm). In this condition, m-Pt nanodots could be aggregated to generate Pt nanoparticles with bigger diameters.

During the thermal treatment, we could observe the generation of mesopores in silica of m-Pt@SiO_2 NPs (Fig. 8a). This is mainly due to the etching of silica in the synthesized m-Pt@SiO_2 NPs in water at high temperature.[35] The etching ability could be related to the degree of condensation of the silica networks due to the dissolution of colloidal silica in water through breaking the Si–O–Si networks and producing mainly monosilicic acid $Si(OH)_4$.[56–58]

In general, one-dimensional arrays of multi-component nanoparticles considerably show the energy transfer characteristics as well as highly efficient catalytic, electronic, and magnetic properties.[59–62] To assemble Pt nanoparticles within a one-dimensional silica matrix for m-Pt@SiO_2 NChs (nanochains), the pH of the reaction media was systematically changed. By changing the pH of the reaction media, we could synthesize m-Pt@SiO_2 NChs with average widths of 15.3 ± 5.5 nm (Fig. 8c). The magnified image of m-Pt@SiO_2 NChs (Fig. 8d) demonstrates that Pt nanodots are placed within the silica NChs. During the synthesis, the presence of H^+ ions in the reaction media of the reverse microemulsion could decrease the amount of OH^- (from NH_4OH), which might decrease the rate of hydrolysis of TEOS and reduce the growth rate of the silica NPs to generate smaller and finally one-dimensional silica structures.[52] This phenomenon mainly originates from the fact that the linear or randomly branched silicone polymers could be generally formed in the acid-catalyzed sol–gel process.[63] Pt nanodots could grow *in situ* while the silica materials generate one-dimensionally to give m-Pt@SiO_2 NChs. Additionally, m-Pt@SiO_2 NChs were successfully synthesized by using highly concentrated EG (18.0 M; Fig. 8e and f). The average width of m-Pt@SiO_2 NChs is 6.8 ± 2.2 nm. Pt nanodots are placed within the silica NChs as could be observed on the magnified image of m-Pt@SiO_2 NChs. Concentrated EG was used as a supplementary reducing agent to further promote the reduction of Pt^{2+} as well as a soft template. The similarity in structural properties of Brij35 and EG,[48–51] which both contain polar –OH functional groups, might result in the strong interaction of those two complexes in a reverse microemulsion. This could lead to the structural change in the reverse micelle, which might be used as a template for m-Pt@SiO_2 NChs. These are interesting examples of how the inorganic nanodots can be assembled within a one-dimensional inorganic oxide matrix, which could show potential use in a vast array of electronic applications.[64–67]

CONCLUSIONS

Platinum (Pt) nanodots assembly core–silica (SiO_2) shells nanosystems (m-Pt@SiO_2 NPs and m-Pt@SiO_2 NChs) were successfully synthesized by a reverse microemulsion (water-in-oil)-based method. The reduction kinetics of K_2PtCl_4 by the Brij35 surfactant were compared in both the presence of reducing agents such as ascorbic acid, glucose, and ethylene glycol and in the absence of supplementary agents within the reverse micelle. To assemble Pt nanoparticles within a one-dimensional SiO_2 matrix for m-Pt@SiO_2 NChs, the pH of the reaction media was systematically changed. For the further usage of mentioned above nanosystems they could be extended to prepare potentially useful catalysts and could be further applied for the plasmon-induced energy transportation, electronics, or modified photosynthesis systems.

ACKNOWLEDGEMENT

This research was supported by the Basic Science Research Program through the National Research Foundation of Korea (NRF) funded by the Ministry of Education, Science and Technology (NRF–2013R1A1A2057675) and by the National Research Foundation of Korea (NRF) grant funded by the Korea government (MSIP; NRF–2015R1A4A10 41631).

REFERENCES

1. T.K. Sau, A.L. Rogach, F. Jäckel, T.A. Klar, and J. Feldmann, *Adv. Mater.* 22, 1805 (2010).
2. C.A. Mirkin, R.L. Letsinger, R.C. Mucic, and J.J. Storhoff, *Nature* 382, 607 (1996).
3. M.R. Jones and C.A. Mirkin, *Nature* 491, 42 (2012).
4. M.M. Maye, I.-I.S. Lim, J. Luo, Z. Rab, D. Rabinovich, T. Liu, and C.-J. Zhong, *J. Am. Chem. Soc.* 127, 1519 (2005).
5. M.M. Maye, J. Luo, I.-I.S. Lim, L. Han, N.N. Kariuki, D. Rabinovich, T. Liu, and C.-J. Zhong, *J. Am. Chem. Soc.* 125, 9906 (2003).
6. A. Roucoux, J. Schulz, and H. Patin, *Chem. Rev.* 102, 3757 (2002).
7. M. José-Yacamán, E. Pérez-Tijerina, and S. Mejía-Rosales, *J. Mater. Chem.* 17, 1035 (2007).
8. H. Lee, S.E. Habas, G.A. Somorjai, and P. Yang, *J. Am. Chem. Soc.* 130, 5406 (2008).
9. R.C. Fox, L.T. Nguyen, L.R. Henshaw, and L. Yu, *ECS Electrochem. Lett.* 2, H40 (2013).
10. A. Fahmi, D. Appelhans, N. Cheval, T. Pietsch, C. Bellmann, N. Gindy, and B. Voit, *Adv. Mater.* 23, 3289 (2011).
11. K.M. Noone and D.S. Ginger, *ACS Nano* 3, 261 (2009).
12. X. Liu, Y. Li, B. Zhou, X. Wang, A.N. Cartwright, and M.T. Swihart, *Chem. Mater.* 26, 3515 (2014).
13. T.-H. Lee, J.I. Gonzalez, J. Zheng, and R.M. Dickson, *Acc. Chem. Res.* 38, 534 (2005).
14. J. Song, J. Zhou, and H. Duan, *J. Am. Chem. Soc.* 134, 13458 (2012).
15. C.-H. Jun, Y.J. Park, Y.-R. Yeon, J. Choi, W. Lee, S. Kob, and J. Cheon, *Chem. Commun.* 1619 (2006).
16. S. Wunder, Y. Lu, M. Albrecht, and M. Ballauff, *ACS Catal.* 1, 908 (2011).
17. L. Zhou, B. He, J. Huang, and A.C.S. Appl, *Mater. Interfaces* 5, 8678 (2013).
18. S.-P. Tai, Y. Wu, D.-B. Shieh, L.-J. Chen, K.-J. Lin, C.-H. Yu, S.-W. Chu, C.-H. Chang, X.-Y. Shi, Y.-C. Wen, K.-H. Lin, T.-M. Liu, and C.-K. Sun, *Adv. Mater.* 19, 4520 (2007).
19. S.E. Lohse and C.J. Murphy, *J. Am. Chem. Soc.* 134, 15607 (2012).
20. J.A. Ascencio, A.C. Rincon, and G. Canizal, *J. Phys. Chem. B* 109, 8806 (2005).

21. B.M. Reddy, A. Khan, P. Lakshmanan, M. Aouine, S. Loridant, and J.C. Volta, *J. Phys. Chem. B* 109, 3355 (2005).
22. Y. Kanda, A. Seino, T. Kobayashi, Y. Uemichi, and M. Sugioka, *J. Jpn. Pet. Inst* 52, 42 (2009).
23. H. Song, R.M. Rioux, J.D. Hoefelmeyer, R. Komor, K. Niesz, M. Grass, P. Yang, and G.A. Somorjai, *J. Am. Chem. Soc.* 128, 3027 (2006).
24. A. Fukuoka, J. Kimura, T. Oshio, Y. Sakamoto, and M. Ichikawa, *J. Am. Chem. Soc.* 129, 10120 (2007).
25. G. Wirnsberger, P. Yang, H.C. Huang, B. Scott, T. Deng, G.M. Whitesides, B.F. Chmelka, and G.D. Stucky, *J. Phys. Chem. B* 105, 6307 (2001).
26. B.J. Scott, M.H. Bartl, G. Wirnsberger, and G.D. Stucky, *J. Phys. Chem. A* 107, 5499 (2003).
27. B.J. Scott, G. Wirnsberger, and G.D. Stucky, *Chem. Mater.* 13, 3140 (2001).
28. X. Gao and S. Nie, *J. Phys. Chem. B* 107, 11575 (2003).
29. L.-N. Sun, H.J. Zhang, C.Y. Peng, J.B. Yu, Q.G. Meng, L.S. Fu, F.Y. Liu, and X.M. Guo, *J. Phys. Chem. B* 110, 7249 (2006).
30. Z. Chang and L. Kevan, *Langmuir* 18, 911 (2002).
31. Y. Zhou, J. Yang, H. Su, J. Zeng, S.P. Jiang, and W.A. Goddard, *J. Am. Chem. Soc.* 136, 4954 (2014).
32. G.-H. Pan, A. Barras, L. Boussekey, R. Boukherroub, and A.C.S. Appl, *Mater. Interfaces* 5, 7042 (2013).
33. J. Wu, H. Zheng, H. Cheng, L. Zhou, K.C. Leong, R. Rajagopalan, H.P. Too, and W.K. Choi, *Langmuir* 30, 2206 (2014).
34. J. Pak and H. Yoo, *J. Mater. Chem. A* 1, 5408 (2013).
35. J. Pak and H. Yoo, *Microporous Mesoporous Mat.* 185, 107 (2014).
36. N.J.C. Ingle, A. Sode, and I. Martens, *Langmuir* 30, 1871 (2014).
37. M. Qamar and A.K. Ganguli, *Bull. Mater. Sci.* 36, 945 (2013).
38. J. Zhou, M. Chena, and G. Diao, *J. Mater. Chem. A* 1, 2278 (2013).
39. H.C. Zeng, *J. Mater. Chem.* 21, 7511 (2011).
40. H. Kitching, M.J. Shiers, A.J. Kenyon, and I.P. Parkin, *J. Mater. Chem. A* 1, 6985 (2013).
41. W. Du, D. Su, Q. Wang, A.I. Frenkel, and X. Teng, *Cryst. Growth Des.* 11, 594 (2011).
42. C. Zhu, S. Guo, and S. Dong, *Adv. Mater.* 24, 2326 (2012).
43. L. Wang, Y. Nemoto, and Y. Yamauchi, *J. Am. Chem. Soc.* 133, 9674 (2011).
44. H. Yoo, J. Sharma, J.K. Kim, A.P. Shreve, and J.S. Martinez, *Chem. Commun.* 47, 2294 (2011).
45. M.H. Jang, J.K. Kim, H. Tak, and H. Yoo, *J. Mater. Chem.* 21, 17606 (2011).
46. M.H. Jang, J.K. Kim, and H. Yoo, *J. Nanosci. Nanotechnol.* 12, 4088 (2012).
47. A.J. Bard, R. Parsons, and J. Jordan, Standard Potentials in Aqueous Solution (Marcel Dekker Inc, New York, 1985), p. 317, 353.
48. A. Zielińska-Jurek, J. Reszczyńska, E. Grabowska, and A. Zaleska, Nanoparticles Preparation Using Microemulsion Systems, Microemulsions—An Introduction to Properties and Applications (InTech, Poland, 2012), p. 235.
49. A.R. Tao, S. Habas, and P. Yang, *Small* 4, 310 (2008).
50. H. Yue, Y. Zhao, X. Ma, and J. Gong, *Chem. Soc. Rev.* 41, 4218 (2012).
51. C. Luo, Y. Zhang, X. Zeng, Y. Zeng, and Y. Wang, *J. Colloid Interface Sci.* 288, 444 (2005).
52. H. Yoo and J. Pak, *J. Nanopart. Res.* 15, 1609 (2013).
53. C.-L. Chang and H.S. Fogler, *Langmuir* 13, 3295 (1997).
54. D. Pant and N.E. Levinger, *Langmuir* 16, 10123 (2000).
55. Y.J. Wong, L. Zhu, W.S. Teo, Y.W. Tan, Y. Yang, C. Wang, and H. Chen, *J. Am. Chem. Soc.* 113, 11422 (2011).
56. Y. Hu, Q. Zhang, J. Goebl, T. Zhang, and Y. Yin, *Phys. Chem. Chem. Phys.* 12, 11836 (2010).
57. G.B. Alexander, W.M. Heston, and R.K. Iler, *J. Phys. Chem.* 58, 453 (1954).
58. T.L. O'Connor and S.A. Greenberg, *J. Phys. Chem.* 62, 1195 (1958).
59. J. Wang, Z.H. Shah, S. Zhang, and R. Lu, *Nanoscale* 6, 4418 (2014).
60. Y. Liu, J. Goebl, and Y. Yin, *Chem. Soc. Rev.* 42, 2610 (2013).
61. Y. Han, Y. Wang, Y. Wang, L. Jiao, and H. Yuan, *Int. J. Hydrog. Energy* 35, 8177 (2010).
62. T.-D. Nguyen and T.-H. Tran, *RSC Adv.* 4, 916 (2014).
63. C.J. Brinker and G.W. Scherer, *Sol-Gel Science: The Physics and Chemistry of Sol-Gel Processing* (Boston: Academic Press, 1990), p. 108.
64. L. Tong, J. Lou, R.R. Gattass, S. He, X. Chen, L. Liu, and E. Mazur, *Nano Lett.* 5, 2 (2005).
65. A.M. Morales and C.M. Lieber, *Science* 279, 208 (1998).
66. W.S. Shi, H.Y. Peng, L. Xu, N. Wang, Y.H.H. Tang, and S.T. Lee, *Adv. Mater.* 12, 1927 (2000).
67. Y. Yin, Y. Lu, Y. Sun, and Y. Xia, *Nano Lett.* 2, 427 (2002).